



## Geodynamics of the Gulf of California from surface wave tomography

Xiaomei Zhang<sup>1</sup>, Hanneke Paulssen\*

Dept. of Earth Sciences, Utrecht University, Utrecht, The Netherlands

### ARTICLE INFO

#### Article history:

Received 17 June 2011

Received in revised form 14 November 2011

Accepted 22 December 2011

Available online 3 January 2012

#### Keywords:

Gulf of California

Surface waves

Tomography

Radial anisotropy

### ABSTRACT

The Gulf of California, which forms part of the Pacific–North American plate boundary, is an ideal place to investigate upper mantle dynamics in a continental rifting area. With 19 seismic stations located around the gulf, the NARS–Baja experiment (2002–2008) was designed to image its crustal and mantle structure. Here we present results of a tomographic inversion of Love and Rayleigh interstation phase velocity measurements for a radially anisotropic shear velocity model of the Gulf of California. This study confirms the overall low shear-wave velocities in the upper 200 km of the mantle found in other Rayleigh wave studies, and the presence of a positive shear-wave velocity anomaly at depths of roughly 80–160 km beneath the central gulf (Zhang et al., 2009). In addition, we find that the horizontal shear velocity ( $V_{SH}$ ) is generally higher than the vertical shear velocity ( $V_{SV}$ ). For the northern gulf, however, there is strong indication for  $V_{SV} > V_{SH}$  in the 40–60 km depth range. This region also has anomalously low shear-wave velocities down to 100 km depth. Combining these observations, we suggest that the low velocity anomaly and the negative radial anisotropy ( $V_{SH} < V_{SV}$ ) beneath the northern gulf are related to vertical flow of low velocity material in an area of a slab window, either by the vertical alignment of olivine crystals or by a fabric of vertically oriented sheets of melt. The high-velocity anomaly beneath the central gulf is interpreted as a remnant slab fragment which inhibits vertical flow from the deeper mantle. Our tomographic results indicate that the formation of the Gulf of California cannot be explained by simple models of crustal extension or dynamic upwelling. Instead, its structure and geodynamics are caused by the cessation of subduction by stalled microplates in the central and southern gulf and the presence of a slab window in the north.

© 2012 Elsevier B.V. All rights reserved.

### 1. Introduction

The Gulf of California is part of the Pacific–North American plate boundary that forms the link between the spreading center of the East Pacific Rise and the San Andreas transform fault. It is a unique plate boundary segment in a region where active convergence between the Farallon and North American plates was replaced by Pacific–North American spreading and transform faulting. In the following we give a brief summary of the tectonic evolution of the region to obtain the perspective of our seismic study.

The Farallon plate subducted beneath North America until ~29 Ma when the Pacific–Farallon spreading ridge reached the trench at the subduction zone. As a consequence, the Pacific plate made direct contact with the North American plate replacing Farallon–North American convergence by Pacific–North American transform motion. With time the contact zone between the Pacific and North-American plate extended to the north and south, and the

Farallon plate fragmented into various microplates (e.g., Lonsdale, 1991; Nicholson et al., 1994; Bohannon and Parsons, 1995; Atwater and Stock, 1998). Two of these, the Guadalupe and the Magdalena microplates, have been identified offshore the Baja California peninsula (Fig. 1). Their subduction beneath Baja California ceased approximately 12 Myr ago. The ridge segment north of these microplates encountered the trench prior to that and locally formed a slab window (Atwater, 1989; Severinghaus and Atwater, 1990). Tectonic reconstructions therefore predict a slab window beneath northern Baja California, whereas Guadalupe and Magdalena slab fragments might be present beneath central and southern Baja California.

When subduction ceased at approximately 12 Ma, the transform motion between the Pacific–North American plates was largely accommodated along the right-lateral San Benito and Toso–Abreojos fault zones which are parallel to the fossil trench (Fig. 1). The extensional component of relative motion was taken up by back-arc extension, forming a proto-Gulf between the Baja California Range to the west and the Sierra Madre Occidental to the east (Spencer and Normark, 1979, 1989). Over time the relative plate motion was increasingly accommodated by strike-slip motion and extension in the proto-Gulf area, the area that became

\* Corresponding author.

E-mail address: [paulssen@geo.uu.nl](mailto:paulssen@geo.uu.nl) (H. Paulssen).

<sup>1</sup> Present address: TNO, Geological Survey of the Netherlands, Utrecht, The Netherlands

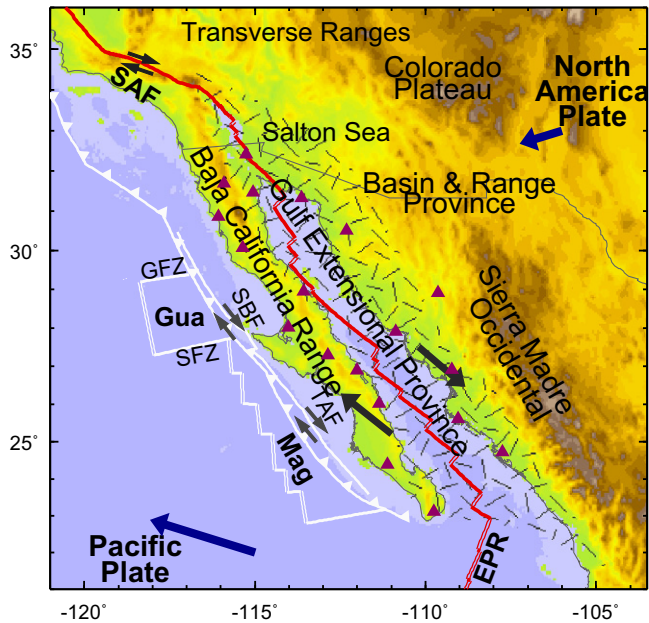


**Fig. 1.** Tectonic map of the Gulf of California region. The main tectonic provinces are the Baja California Range, Gulf Extensional Province (hatched) and the Sierra Madre Occidental. The present day plate boundary is shown in red, inactive plate boundaries are shown as white lines. Arrows indicate plate motions: absolute plate motions in blue (HS3-NUVEL1A, Gripp and Gordon, 2002), relative plate motion in grey. Abbreviations: SAF, San Andreas Fault; EPR, East Pacific Rise; Gua, Guadalupe Microplate; Mag, Magdalena Microplate; SBF, San Benito Fault; TAF, Tosco Abreojos Fault; GFZ, Guadalupe Fracture Zone; SFZ, Shirley Fracture Zone.

the Gulf Extensional Province (Stock and Hodges, 1989). At approximately 6 Ma, most of the Pacific–North American transform motion along the San Benito and Tosco-Abreojos faults ended, moved inland, and was taken over by transform faults and pull-apart basins in the proto-Gulf area (e.g., Lonsdale, 1991; Oskin and Stock, 2003). Consequently, the Gulf of California started to open. Currently, approximately 90% of the Pacific–North American plate motion (of 51 mm/yr) is taken up by northwest extension in the gulf (Plattner et al., 2007).

Although many aspects of the tectonic evolution are known, the processes that caused the opening of the gulf remain elusive and the current geodynamics of the region is unclear. An intriguing aspect is, for instance, that there are structural differences in the style of rifting along the Gulf of California. It changes character from an oceanic-type spreading centre and transform fault system in the South to a region of diffuse continental extensional deformation in the North (Lonsdale, 1989; Nagy and Stock, 2000; González-Fernández et al., 2005). Furthermore, the basins in the southern and central gulf change from wide to narrow rifts over distances of only ~200 km (Lizarralde et al., 2007). The causes of these variations are poorly understood.

The NARS-Baja experiment (Trampert et al., 2003, Fig. 1) with 19 broadband seismic stations deployed around the Gulf of California (2002–2008) was designed to study the seismicity and mantle structure beneath the gulf. Previous studies using these data have already provided some important results. Persaud et al. (2007) determined the crustal thickness under the NARS-Baja stations from receiver functions and found eastward crustal thinning of the Baja California peninsula. Using SKS splitting Obrebski et al. (2006), van Benthem et al. (2008), and Long (2010) found strong lateral variations in upper mantle anisotropy that they associated with past Farallon subduction and absolute plate motion directions. Strong structural variations, potentially related to the presence of stalled Farallon slab fragments, were also inferred by Obrebski and Castro (2008) from anisotropic receiver function

analyses of three NARS-Baja stations. Several surface wave studies provided information about the shear velocity structure (López-Pineda et al., 2007; Zhang et al., 2007; Zhang et al., 2009; Wang et al., 2009). The Rayleigh wave tomographic study of Zhang et al. (2009) showed for the first time the presence of a relatively high velocity anomaly at depths of more than ~100 km. They interpreted this anomaly as a remnant slab fragment beneath the central part of the gulf. More shallow (50–90 km) local low velocity anomalies on the other hand suggest small scale dynamic upwelling beneath the gulf (Wang et al., 2009).

In this study we inverted interstation Love and Rayleigh wave phase-velocity curves for the radially anisotropic shear velocity structure of the gulf. Features of the isotropic shear velocity structure and variations in radial anisotropy in the uppermost mantle show that the imprint of the tectonic history is still visible in the shallow mantle structure which may explain the variations in rifting along the gulf.

## 2. Method and data

Using data from the NARS-Baja experiment, we constructed a shear velocity model with radial anisotropy beneath the Gulf of California by a three stage inversion. In the first stage, we measured phase velocities of the fundamental mode Love and Rayleigh waves between the station pairs of the NARS-Baja network. In the second step the measured dispersion curves were inverted for 2-D phase-velocity maps at different periods for each of the two wave-types. As a result, we estimated at each geographical location the local Love and Rayleigh wave phase velocity curves. In the third step these dispersion curves were inverted for radially anisotropic 1-D shear wave velocity models which were combined into a 3-D radially anisotropic shear-velocity model.

### 2.1. Interstation phase velocity measurements

In the first stage, the phase velocities of the fundamental mode Love and Rayleigh waves were measured for paths between the stations of the NARS-Baja network across and around the gulf (see Fig. 2).

The interstation approach is based on the assumption that surface waves propagate along the great-circle path so that the dispersion curves are representative of the structure between the two stations. From the cross-correlation function of two vertical (or transverse) component seismograms, excited by the same event recorded at two stations with the same back azimuth, one can find the Rayleigh (or Love) wave phase velocity  $c$  at frequency  $\omega$  (Sato, 1955):

$$c(\omega) = \frac{\omega(\Delta_1 - \Delta_2)}{\arctan(\text{Im}[\Phi(\omega)]/\text{Re}[\Phi(\omega)]) + 2n\pi},$$

where  $\Phi(\omega)$  is the cross-correlation function of the two seismograms at frequency  $\omega$ ,  $\text{Re}[\Phi(\omega)]$  and  $\text{Im}[\Phi(\omega)]$  are the real and imaginary components of  $\Phi(\omega)$  respectively,  $\Delta_1$  and  $\Delta_2$  the epicentral distances, and the indices 1 and 2 refer to the two stations. Because of the  $2\pi$ -ambiguity of the arctan function, the phase velocity is estimated from an array of curves for different values of  $n$ , where  $n$  is an integer.

Following the approach of Meier et al. (2004), we measured phase velocities of fundamental mode Rayleigh (or Love) waves by cross-correlating vertical (or transverse) component displacement seismograms from two stations. The displacement fields are excited by events located up to  $7^\circ$  from the great circle between the two stations. A  $7^\circ$  difference corresponds to a 1% difference in phase velocity, which is generally smaller than the uncertainty caused by scattering, multipathing, off-great circle propagation,

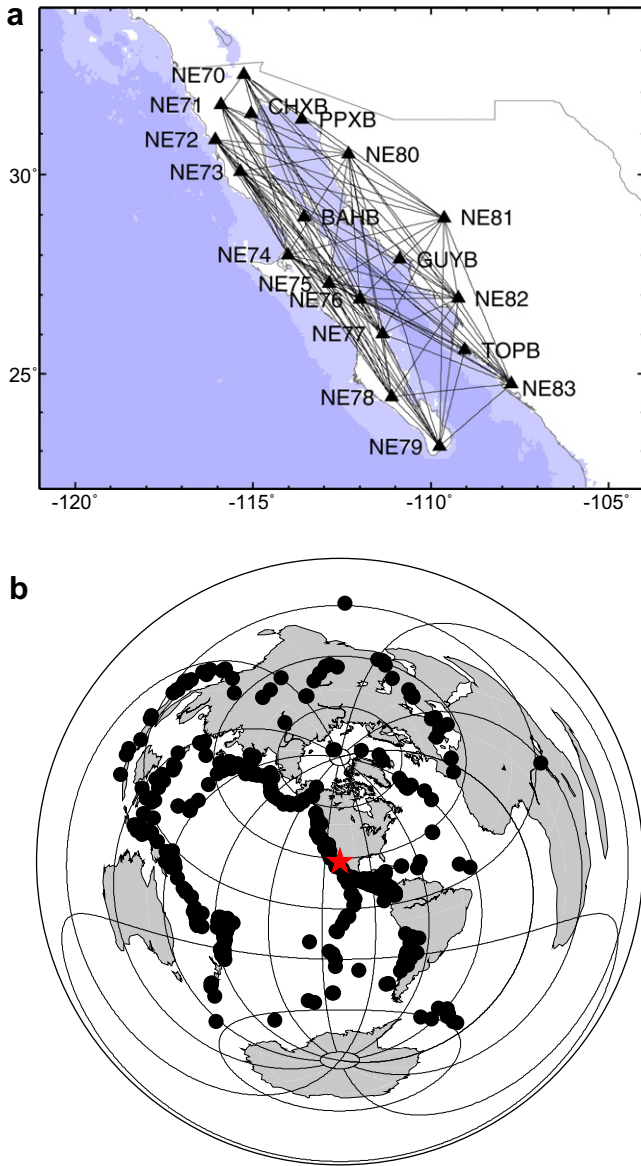


Fig. 2. (a) Stations and interstation path coverage. (b) Event distribution.

i.e. various types of finite frequency effects. The method involves frequency-dependent filtering and weighting, and the phase velocity curve is interactively selected in the frequency domain. Only the best (parts of the) phase velocity curves were selected and inconsistent measurements were discarded. More details about the approach can be found in Meier et al. (2004) and Zhang et al. (2007, 2009). For each path, the final phase velocity curve was obtained as the average of at least eight individual curves with a minimum of four measurements per period. However, in most cases we had more than 20 phase velocity curves per path. The uncertainty was taken as  $\pm 1$  standard deviation from the average of the ensemble of curves.

The Love wave data set consists of 2077 transverse component seismograms excited by 461 earthquakes with moment magnitudes larger than 5. In total, we obtained 92 interstation phase-velocity dispersion curves of the fundamental mode Love wave. Fig. 2 shows the distribution of the events as well as the locations of the stations and path distribution. The Rayleigh wave dispersion curves for the same paths were taken from Zhang et al. (2009). The Rayleigh wave data set includes 5292 vertical component waveforms of 858 earthquakes with a moment magnitude larger than

5. Fig. 3 shows the number of paths at different periods of the interstation phase velocity measurements. Although the same paths were selected for the two data sets, the path distribution of the Love and Rayleigh wave measurements varies for the different periods. At longer periods there are more Rayleigh than Love wave measurements. This is due to the greater difficulty in measuring Love waves at long periods and the higher noise level on the transverse component seismograms. The reduced Love-wave path coverage at long periods limits the resolution of the shear-wave velocity model at larger depths.

## 2.2. Love and Rayleigh phase velocity maps

In the second stage, the two sets of 92 interstation phase velocity measurements are inverted for Love and Rayleigh phase velocity maps that include azimuthal anisotropy. The inversion of a set of interstation phase velocity dispersion curves to phase velocity maps at individual periods can be solved as a linear problem. At a given period, the interstation phase velocity perturbation  $d$  for path  $i$  with an azimuth  $\psi$  is

$$d_i = \sum_{j=1}^m K_{ij} \delta C_j = \sum_{j=1}^m K_{ij} (\delta C_{(iso)j} + \delta A_{(2\psi)j} \cos 2\psi + \delta B_{(2\psi)j} \sin 2\psi + \delta A_{(4\psi)j} \cos 4\psi + \delta B_{(4\psi)j} \sin 4\psi),$$

where  $K_{ij}$  is the weight of grid point  $j$  to path  $i$ , determined by the relative position between the grid point and the path (Lebedev and van der Hilst, 2008), and  $m$  is the number of grid points on the phase velocity map. The five coefficients  $\delta C_{(iso)j}$ ,  $\delta A_{(2\psi)j}$ ,  $\delta B_{(2\psi)j}$ ,  $\delta A_{(4\psi)j}$  and  $\delta B_{(4\psi)j}$  describe the phase velocity perturbations  $\delta C_j$  at each geographical grid point, obtained as a first-order approximation for a plane layered medium with weak general anisotropy (Smith and Dahlen, 1973): the coefficient  $\delta C_{(iso)j}$  is the isotropic phase velocity perturbation;  $\delta A_{(2\psi)j}$ ,  $\delta B_{(2\psi)j}$ ,  $\delta A_{(4\psi)j}$  and  $\delta B_{(4\psi)j}$  parameterize azimuthal anisotropy. In this study we adopted a similar approach to that of Lebedev and van der Hilst (2008) to solve this linear inverse problem. The five phase velocity perturbation coefficients, at the knots of a triangular grid with a nearly-uniform spacing of 100 km, were inverted by using LSQR (Paige and Saunders, 1982) with smoothing and slight norm damping.

We used the same damping and smoothing factors in this step as in Zhang et al. (2009), a relatively strong smoothing and only slight norm damping, to obtain robust albeit rather smooth phase velocity maps. The same regularization was used for all periods to avoid lateral variations in the phase velocity maps caused by variations in damping and smoothing. The resolution matrices were calculated and various resolution tests were carried out to analyze the robustness of the results. An example of a resolution matrix is shown in Supplementary material. Fig. 4 gives an indication of the resolution in the final phase velocity maps. The colour at each grid point marks the resolution of the isotropic term by the value of the diagonal element in the resolution matrix. The directional distribution represents the azimuthal path coverage. We found that the isotropic components were much better resolved than the anisotropic components, and the resolution length for the isotropic structure is estimated to be 150–200 km in the best resolved area, i.e. in the gulf. Figures showing the lateral resolution for two grid points in the gulf can be found in Supplementary material. The anisotropic components have a relatively poor resolution; especially the anisotropic terms of the Love waves at longer periods were poorly resolved due to the reduced azimuthal coverage. As one of the tests, we calculated resolution matrices for inversions with and without the anisotropic terms. We found that the isotropic terms were scarcely affected by the inclusion of the anisotropic terms.

The Love and Rayleigh phase-velocity maps of the inversion at various periods are shown in Fig. 5 with an indication of the region

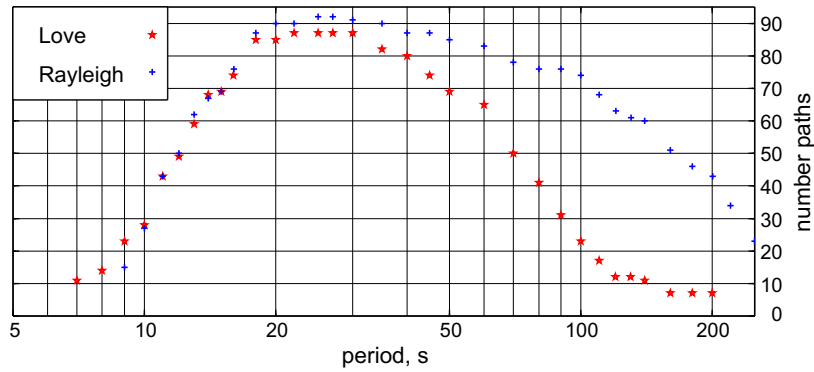


Fig. 3. Number of Love and Rayleigh wave paths at different periods for the interstation phase velocity measurements.

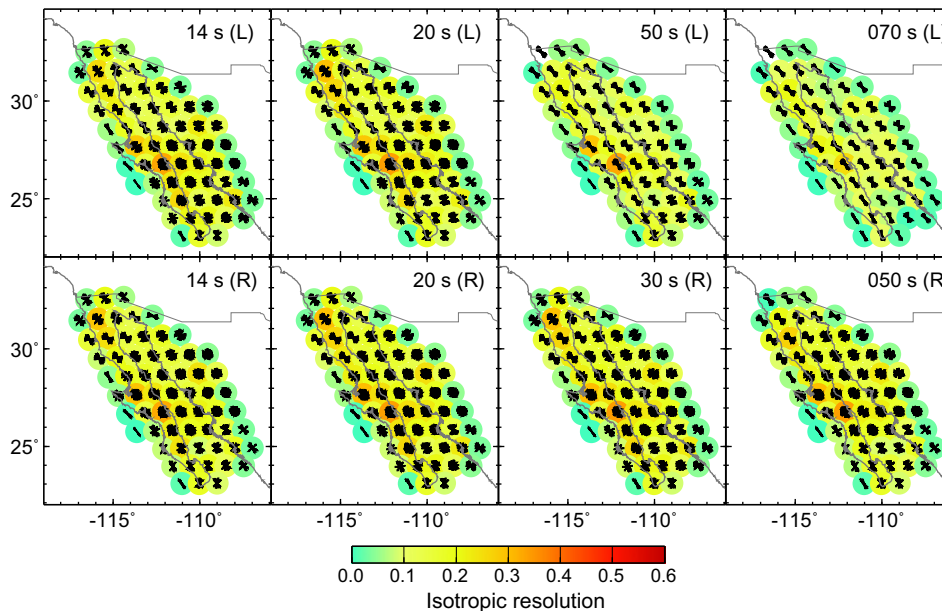


Fig. 4. Resolution maps. The round dots indicate the grid points used to parameterize the inversion with the colour representing the size of the diagonal element of the isotropic term of the resolution matrix. The black bars indicate the azimuth distribution of the paths contributing to the phase velocity at each grid point.

of good resolution, which is defined as having a value larger than 0.1 for the diagonal element of the isotropic term of the resolution matrix. All  $\chi^2$  misfits were less than 1, with most values ranging between 0.6 and 0.7, which means that the data were fitted within their uncertainty.

### 2.3. Depth inversion

In the third and last stage of the inversion, the isotropic parts of the phase velocity models were used to construct a radially anisotropic shear-velocity structure. For this, the local Love- and Rayleigh-wave phase velocity curves at all grid points were inverted for 1-D radially anisotropic shear-velocity models, which were then combined to form the 3-D shear-velocity structure.

A transversely isotropic medium with a vertical axis of symmetry, is described by density  $\rho$  and the five Love coefficients ( $A$ ,  $C$ ,  $F$ ,  $L$  and  $N$ ) (Love, 1927). However, from horizontally travelling Love waves we can only reliably estimate the horizontally polarized shear wave velocity ( $V_{SH} = \sqrt{N/\rho}$ ), and from Rayleigh waves, the vertically polarized shear wave velocity ( $V_{SV} = \sqrt{L/\rho}$ ).

Taking the isotropic terms of the phase velocities from the second stage, we performed a point-by-point depth inversion to constrain the radially anisotropic shear wave velocity structure. For

each geographical grid point, we inverted Love- and Rayleigh-wave dispersion curves simultaneously for the average shear wave velocity,  $V_S = (V_{SH} + V_{SV})/2$ , and the amount of radial anisotropy,  $V_{SH} - V_{SV}$ . The inversion is performed by the Levenberg-Marquardt algorithm where at each iteration the Love and Rayleigh wave phase velocities are recomputed from the perturbed shear-wave velocity model. The compressional velocity  $V_P$  was assumed to be isotropic with its perturbation coupled to  $V_S$  as  $d \ln V_S / d \ln V_P = 1.7$ . The density was kept constant in the inversion.

It is important to have a good starting model in the inversion, especially of the Moho depth, because an incorrect Moho depth can bias the crustal and uppermost mantle structure and result in improper estimates of radial anisotropy (Levshin and Ratnikova, 1984; Bozdogan and Trampert, 2008; Ferreira et al., 2010). We used the crustal model of Zhang et al. (2009) which was constructed from a local velocity model in southern California (Süss and Shaw, 2003), seismic refraction lines in the gulf (González-Fernández et al., 2005; Lizarralde et al., 2007), receiver functions (Lewis et al., 2001; Persaud et al., 2007), and crustal model CRUST2.0 (Basin et al., 2000). For more details about the crustal starting model see Zhang et al. (2009). This 3-D a priori crustal model for the Gulf of California region was combined with the mantle velocity structure of model AK135 (Kennett et al., 1995) to form 1-D isotropic

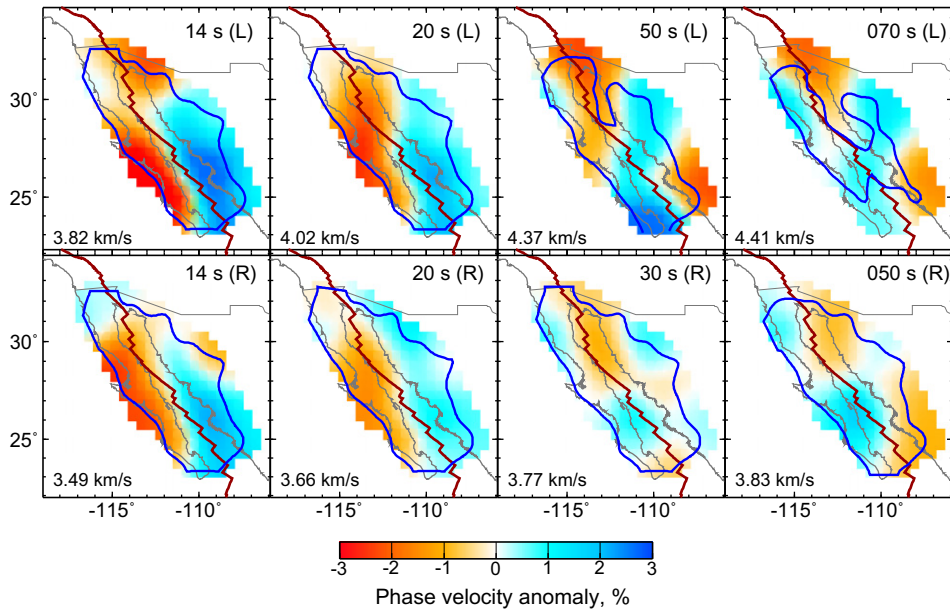


**Fig. 5.** Tomographic maps of Love and Rayleigh wave phase velocities at different periods. The period is shown in the upper right corner and the reference phase velocity is in the lower left corner of each panel. The colours indicate the isotropic phase velocity anomalies. The thick red line marks the location of the plate boundary. The blue contour delineates the region of high resolution (with diagonal element of the isotropic term of the resolution matrix  $>0.1$ ).

starting models for all 63 grid points. In the inversions, the Moho depth was allowed to vary, as well as the 410 and 660-km discontinuities. The shear wave velocity perturbations to a depth of 1000 km were expanded using 12 basis functions. Of these, one is boxcar in shape spanning the crust, and 11 triangular basis functions were used to parameterize the mantle structure with denser sampling at shallower depths.

For each grid point, there are many radially anisotropic shear wave velocity models which fit the Love and Rayleigh dispersion data within the 0.5% estimated uncertainty. The model obtained from the inversion, i.e. the size of the average shear-velocity anomaly and the amount of radial anisotropy, depends strongly on the damping. We tested different amounts of damping, and the final model presented here is very conservative on radial anisotropy: the amount of radial anisotropy,  $V_{SH}-V_{SV}$ , is damped stronger to zero than the average shear-velocity perturbation. The amount of radial anisotropy was therefore forced to be small.

### 3. Radially anisotropic shear-wave velocity structure

The radially anisotropic shear-wave velocity structure as obtained from the inversion is presented in Figs. 6 and 7. Since the period range of the Love wave phase velocity data (see Fig. 3) is limited, providing a sensitivity mainly above 200 km, we only show the upper 200 km of the model. It should also be noted that the shear velocity structure is less well constrained at the edges of the model due to larger uncertainties in the phase velocity maps. We therefore focus our interpretation on the Gulf of California.

Fig. 6 shows the shear wave velocity anomalies at various depths as percentage of the average velocity at that depth. The shear wave velocity structure ( $V_S$ ) shows many similarities to the  $V_{SV}$ -structure inferred from Rayleigh waves for the extended area of Zhang et al. (2009) and the Rayleigh wave study of Wang et al. (2009). All studies, including the one by Zhang et al. (2007), indicate that the Gulf of California is characterized by low velocities compared to the global average to depths of at least 200 km. In the uppermost mantle (40–50 km) the low velocities are mainly confined to the gulf area. The low velocities in the 40–100 km

depth range probably require, at least locally, the presence of melt (Stixrude and Lithgow-Bertelloni, 2005; Afonso et al., 2008). Wang et al. (2009) found three distinct low-velocity anomalies beneath the northern and central gulf in the 40–90 km depth range which they interpret as regions of dynamic upwelling by partial melting. We also find low-velocity anomalies at more or less similar locations, but found that their magnitude, and lateral and depth extend depend on the regularization and parameterization of the inversion. Our approach in constructing the phase velocity maps and the subsequent shear-velocity inversion is more conservative to avoid overinterpretation of the results.

Our results show a high velocity anomaly beneath the central part of the gulf ( $\sim 27^\circ\text{N}$ ,  $\sim 111^\circ\text{W}$ ) at depths roughly between 80 and 160 km. This anomaly was first imaged by Zhang et al. (2009) and was interpreted as a detached slab remnant beneath central Baja California. The presence of such a slab fragment had already been suggested based on tectonic modelling (Bohannon and Parsons, 1995), volcanic evidence (e.g., Benoit et al., 2002, 2004, 2005, 2007), and bathymetric and magnetic data offshore Baja California (Michaud et al., 2006), although interpretations about the process of slab detachment vary. The high velocities beneath the southern Baja California peninsula (south of  $26^\circ\text{N}$ ), at depths between 60 and 100 km, may be linked to the Magdalena microplate offshore.

In contrast to the central gulf, the shear-wave velocities beneath the northern gulf remain very low to depths of at least 100 km, certainly when compared to the global average. The northern Gulf of California is a region with a suggested slab window (Dickinson and Snyder, 1979; Severinghaus and Atwater, 1990; Dickinson, 1997). This is a slabless region beneath the continent that forms within a subduction zone after the arrival of a ridge segment at the trench.

The new aspect of the current study is the determination of radial anisotropy from the combination of Love and Rayleigh wave phase velocity data. Fig. 7 shows the radial anisotropy,  $(V_{SH}-V_{SV})/V_S$ , as obtained from the inversion. Note that it is a conservative model due to the strong damping that is applied to the anisotropy. The pattern is therefore more meaningful than the amplitude of

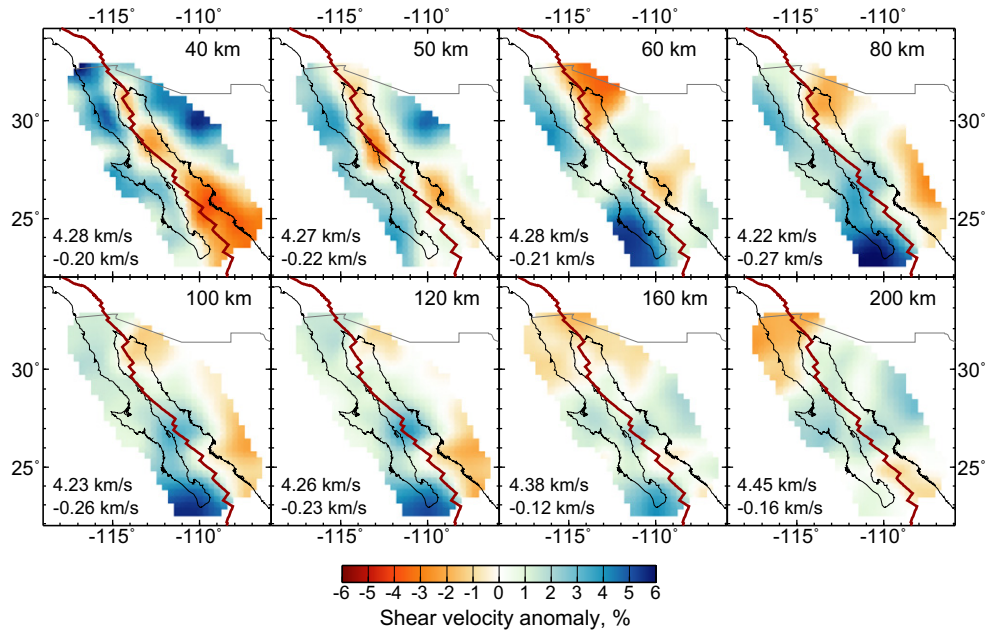


**Fig. 6.** Maps of shear wave velocity structure ( $V_s = (V_{SH} + V_{SV})/2$ ) at different depths. The depth is indicated in the upper right corner and the reference shear wave velocity in the lower left corner together with its difference to model AK135 at that depth.

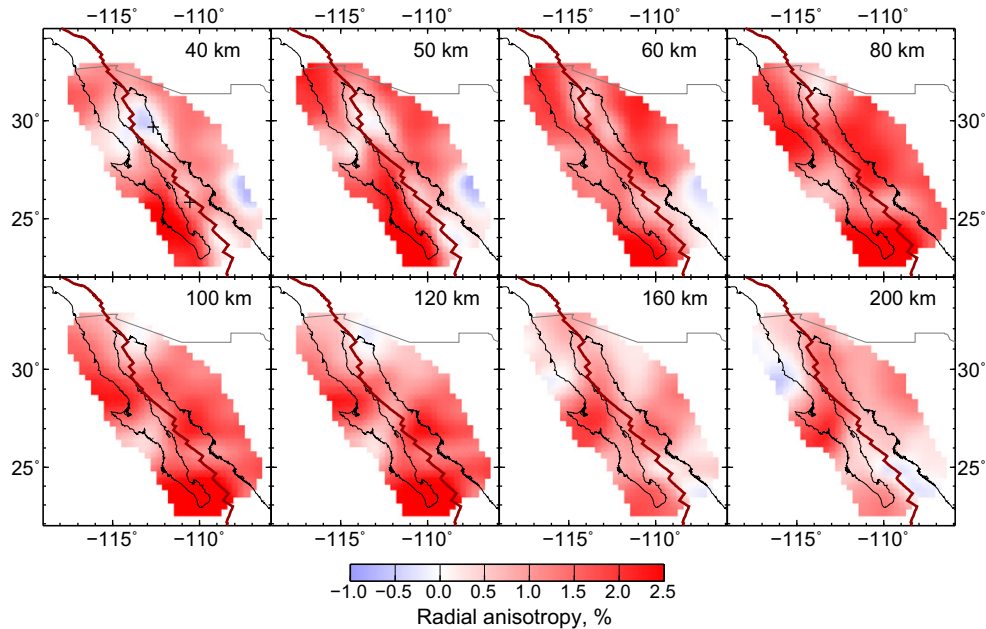


**Fig. 7.** Maps of percentage of radial anisotropy ( $(V_{SH} - V_{SV})/V_s$ ) at different depths. The depth is indicated in the upper right corner. The locations of the two nodes investigated by Monte Carlo simulations are marked by the plus signs in the 40-km depth map.

the anomalies. Furthermore, the maps of radial anisotropy are more uncertain for depths larger than 100 km because of the unbalance of Love and Rayleigh wave data at greater depths (less Love wave data at longer periods) and differences in their sensitivity kernels. We therefore refrain from interpreting the radial anisotropy below 100 km.

Overall, the model has positive radial anisotropy,  $V_{SH} > V_{SV}$ , with the radial anisotropy increasing (becoming more positive) from 40 to 100 km depth for the area within gulf. In addition, the radial anisotropy is smaller beneath the northern and southern gulf than beneath the central gulf. In spite of the strong damping applied on the anisotropic term, the model even has negative radial

anisotropy ( $V_{SH} < V_{SV}$ ) in northern gulf in the 40–60 km depth range for latitudes between 28° and 31°N. An inversion with less damping shows the anomaly much more clearly with an amplitude of up to 5%. The model is obviously non-unique, and the robustness of the anomaly in the northern gulf was therefore further investigated. Several Monte Carlo searches were carried out for two selected grid points, one in the northern and one in the central-southern gulf (see Fig. 7).  $V_{SH}$  and  $V_{SV}$  were allowed to vary within 5% from the average  $V_s$  model obtained for each grid point and different mantle parameterizations were used in different Monte Carlo tests. Because the crustal structure has a strong effect on the inferred upper mantle radial anisotropy, we not only allowed the

average crustal velocity structure to vary by  $\pm 5\%$  but also the Moho depth by  $\pm 3$  km. The accepted models fitted the Love and Rayleigh wave phase velocity curves everywhere within boundaries of  $\pm 1\%$ . At least 65% of the accepted models per Monte Carlo test had  $V_{SH} < V_{SV}$  in the  $\sim 40$ – $60$  km depth range for the northern grid point, whereas for other depths  $V_{SH} > V_{SV}$  for the majority of the models. For the other grid point such a distinction is not clear. The results of one such a set of Monte Carlo tests are shown in [Supplementary material](#). The accepted models further showed that there is an overall tendency for  $V_{SH} > V_{SV}$  although this is hardly constrained for depths larger than 100 km. This larger uncertainty at larger depths is due to the reduced data coverage of Love waves at long periods, and we therefore do not interpret these results.

#### 4. Interpretation and discussion

Seismic anisotropy in the upper mantle is believed to be predominantly an effect of the lattice preferred orientation (LPO) of mantle minerals and mainly olivine (e.g., [Estey and Douglas, 1986](#); [Karato, 1989](#); [Montagner, 1998](#)). Therefore, it has often been used to infer the deformation geometry of the Earth's upper mantle (e.g., [Montagner, 2002](#); [Marone et al., 2007](#); [Visser et al., 2008](#)). Under the assumption that the fast axis of olivine aligns with the flow direction for A-type of olivine fabric ([Nicolas and Christensen, 1987](#)), radial anisotropy with  $V_{SH} > V_{SV}$  is often interpreted as evidence of horizontal flow, whereas  $V_{SH} < V_{SV}$  is generally related to vertical flow.

However, recent studies on mineral physics and petrological observations have revealed that other types of olivine fabric can exist in the upper mantle. Therefore, the relationship between seismic anisotropy and LPO is more complex and depends on the presence of water, as well as on stress, temperature and pressure conditions (e.g., [Jung and Karato, 2001](#); [Mainprice et al., 2005](#); [Karato, 2008](#); [Jung et al., 2009](#)). These studies show that the A-type fabric is only present in depleted water-poor regions like the lithosphere, except in local high-stress regions where the D-type fabric will develop. In undepleted regions with a moderate to high water content, such as subduction zones, plumes or deep asthenosphere, other types of olivine fabrics (B-, C-, or E-type) may exist. With these, the relationship between anisotropy and the flow direction can be different from those of A-type. For an overview of the olivine fabrics and their relation to flow see [Karato et al. \(2008\)](#).

Our results suggest that the percentage of radial anisotropy increases with depth in the upper 100 km of the mantle beneath the gulf. If only A-type LPO of olivine is present, this means that the horizontal alignment of the minerals would increase with depth. This could be explained by a gradual change in the flow direction with a larger component of horizontal flow at larger depth, or, stated differently, a larger component of vertical flow in the more shallow upper mantle.

The amount of anisotropy also changes along the strike of the gulf.  $(V_{SH}-V_{SV})/V_S$  is negative or small beneath the northern gulf and at the mouth of the gulf, whereas it is positive in the central gulf, right above the high  $V_S$  anomaly. If we only consider A-type LPO of olivine, this would imply that there is stronger vertical flow in the 40–60 km depth range of the northern gulf, i.e. in the region of the slab window, than in the mantle above the slab fragment. If other olivine fabrics exist in the upper mantle beneath the Gulf of California, the interpretation could be different. However, B- or E-type fabrics would produce  $V_{SH} > V_{SV}$  for horizontal flow as well, with E-type giving a smaller amplitude. Therefore, the presence of B- and/or E-type fabrics would lead to the same interpretation as above. The C-type would lead to a different interpretation, but this fabric needs a high water content and low stress environment ([Karato et al., 2008](#)). A high water content might exist in the upper

mantle above the slab remnant in the central gulf as a result of slab dehydration. It would then give  $V_{SV} > V_{SH}$  in case of horizontal flow, which is not observed, or only weak  $V_{SH} > V_{SV}$  in case of vertical cylindrical flow ([Karato et al., 2008](#)).

An alternative explanation is that the anisotropy is a result of shape preferred orientation (SPO), such as fine layering or preferred alignment of melt inclusions. For instance, a stack of thin horizontal layers produces an effective anisotropy with  $V_{SH} > V_{SV}$ , whereas vertically aligned melt sheets give  $V_{SV} > V_{SH}$ . The effects of melt may be even more complicated as [Holtzman et al. \(2003\)](#) showed that, under shear, small amounts of partial melt in mantle rock may segregate to form networks of weak shear zones which separate relatively melt-free bands containing olivine fabric. Thus the effective anisotropy for a rock with partial melt is a combination of anisotropy due to LPO and the alignment of melt pockets and melt rich bands. Recently, [Holtzman and Kendall \(2010\)](#) modelled these combined and related effects to explain the differences in observed anisotropy for different divergent plate boundary settings. Their results require steeply dipping melt rich bands to explain  $V_{SV} > V_{SH}$  and more horizontally layered melt structures for  $V_{SH} > V_{SV}$ . Assuming such melt segregation processes in the Gulf of California, this would imply more steeply aligned melt structures for the northern gulf, and more horizontal layering in the central gulf. In summary, whether due to LPO or SPO, the radial anisotropy is most likely explained by upwelling in the northern slab window, and more horizontal flow in the central gulf above the slab remnant. This may imply that the slab acts as a barrier to the vertical ascent of deeper mantle material.

Additional information on mantle flow can be obtained from azimuthal anisotropy. The Rayleigh wave phase velocity maps of ([Zhang et al., 2009](#), see their [Fig. 4](#)) can be used for this purpose. In the gulf region, at a period of 30 s, with a main sensitivity below the crust, the  $2\psi$  Rayleigh wave azimuthal anisotropy is smaller than at periods of 50 and 80 s. This agrees with our interpretation of increasing horizontal flow at larger mantle depths. Furthermore, the long period (50–100 s) surface wave data and the SKS splitting studies by [Obrebski et al. \(2006\)](#), [van Benthem et al. \(2008\)](#) and [Long \(2010\)](#), show roughly E–W fast directions for the stations in the North, whereas other Rayleigh wave fast directions and small SKS delay times and null measurements are dominant in the central and southern part of the peninsula. The change in pattern seems related to the presence of the slab remnant and coincides with the change in the radially anisotropic structure revealed in our study. Indeed, [van Benthem et al. \(2008\)](#) and [Long \(2010\)](#) suggested that their observations of low anisotropy may be caused by subducted microplate fragments. The splitting data, however, do not have much depth resolution ([Sieminski et al., 2008](#)).

Finally, the major change in style of rifting along the gulf is found to be consistent with the variations in our 3-D model. The northern gulf is characterized by diffuse continental deformation, whereas the central and southern gulf are oceanic in character with oceanic-type spreading centers and transform faults ([Nagy and Stock, 2000](#)). Moreover, the crustal thickness varies from more than 14 km below the northern gulf ([González-Fernández et al., 2005](#)) to less than 10 km below the central-southern gulf ([Lizarralde et al., 2007](#)). We suggest that these variations may be related to changes in melt composition and mantle flow pattern as a consequence of the presence of a slab window in the north and a slab fragment in the central-southern gulf.

#### 5. Conclusion

This model of the upper mantle below the Gulf of California shows lateral variations that can be related to the presence of a slab window in the northern gulf and a remnant slab fragment in

the central gulf. The northern gulf shows lower shear velocities in the 40–80 km depth range than the already low averages for the entire gulf area. Furthermore, there is a strong indication for  $V_{SV} > V_{SH}$  that may be caused by vertical alignment of the olivine  $a$ -axes (A-type LPO) or by vertically aligned melt bands. Both of these mechanisms are suggestive of a dominant component of vertical flow in the slab window. More to the south, in the central gulf, the relatively high velocity anomaly at ~80–160 km depth is associated with the presence of a remnant slab fragment. This slab fragment may act as a barrier to vertical flow from the deeper mantle, which may explain why we do not find negative radial anisotropy ( $V_{SH} - V_{SV} < 0$ ) in the shallow mantle above the slab fragment. Instead, the positive radial anisotropy may be caused by horizontal alignment of olivine  $a$ -axes or fine horizontal layering, suggestive of a more horizontal flow direction. The differences in the radially anisotropic shear-wave velocity structure indicate small scale variations in flow pattern that are related to past subduction of Farallon microplates. Simple models of passive rifting by lithospheric extension or dynamic rifting by buoyant flow do not explain all aspects of the structure and evolution of the Gulf of California. From this study we therefore infer that the recent subduction history still plays a key role in the local geodynamics of the area.

## Acknowledgments

We thank all people who supported the NARS-Baja project, and in particular the technical support by Arie van Wettum and Arturo Perez-Vertti. Funding for this project was provided by Utrecht University, the Netherlands Organisation for Scientific Research (NWO, Grant NWO-GOA 750.396.01) and the US National Science Foundation (Grant EAR-0111650 of the Margins program). We also thank two reviewers for constructive comments that helped to improve the paper.

## Appendix A. Supplementary data

Supplementary data associated with this article can be found, in the online version, at [doi:10.1016/j.pepi.2011.12.001](https://doi.org/10.1016/j.pepi.2011.12.001).

## References

- Afonso, J.C., Fernández, M., Ranalli, G., Griffin, W.L., Connolly, J.A.D., 2008. Integrated geophysical-petrological modelling of the lithosphere and sublithospheric upper mantle: methodology and applications. *Geochim. Geophys. Geosyst.* 9, Q05008. doi:10.1029/2007GC001834.
- Atwater, 1989. Plate tectonic history of the northeast Pacific and western North America. In: Winterer, E.L., Hussong, D.M., Decker, R.W. (Eds.), *The Eastern Pacific Ocean and Hawaii, The Geology of North America*, volume N, pp. 499–521.
- Atwater, T., Stock, J.M., 1998. Pacific–North America plate tectonics of the Neogene Southwestern United States: an update. *Int. Geol. Rev.* 40, 375–402.
- Bassin, C., Laske, G., Masters, G., 2000. The current limits of resolution for surface wave tomography in North America. *EOS Trans. AGU* 81, F897.
- Benoit, M., Aguillón-Robles, A., Calmus, T., Maury, R., Bellon, H., Cotten, J., Bourgois, J., Michaud, F., 2002. Geochemical diversity of Late Miocene volcanism in southern Baja California, Mexico: implication of mantle and crustal sources during the opening of an asthenospheric window. *J. Geol.* 110, 627–648.
- Bohannon, R.G., Parsons, T., 1995. Tectonic implications of post-30 Ma Pacific and North American relative plate motions. *Geol. Soc. Am. Bull.* 107, 937–959.
- Bozdogan, E., Trampert, J., 2008. On crustal corrections in surface wave tomography. *Geophys. J. Int.* 172, 1066–1082. doi:10.1111/j.1365-246X.2007.03690.x.
- Conly, A., Brenan, J., Bellon, H., Scott, S., 2005. Arc to rift transitional volcanism in the Santa Rosalía Region, Baja California Sur, Mexico. *J. Volcanol. Geotherm. Res.* 142, 303–341.
- Dickinson, W.R., 1997. Tectonic implications of Cenozoic volcanism in coastal California. *Geol. Soc. Am. Bull.* 109, 936–954.
- Dickinson, W., Snyder, W., 1979. Geometry of triple junctions related to San Andreas transform. *J. Geophys. Res.* 84, 561–572.
- Estey, L.H., Douglas, B.J., 1986. Upper mantle anisotropy: a preliminary model. *J. Geophys. Res.* 91, 11393–11406.
- Ferrari, L., 2004. Slab detachment control on mafic volcanic pulses and mantle heterogeneity in central Mexico. *Geology* 32, 77–80.
- Ferreira, A.M.G., Woodhouse, J.H., Visser, K., Trampert, J., 2010. On the robustness of global radially anisotropic surface wave tomography. *J. Geophys. Res.* 115, B04313. doi:10.1029/2009JB006716.
- Gripp, A.E., Gordon, R.G., 2002. Young tracks of hotspots and current plate velocities. *Geophys. J. Int.* 150, 321–361.
- González-Fernández, A., Dañoibeitia, J.J., Delgado-Argote, L.A., Michaud, F., Córdoba, D., Bartolomé, R., 2005. Mode of extension and rifting history of upper Tiburón and upper Delfin basins, northern Gulf of California. *J. Geophys. Res.* 110, B01313. doi:10.1029/2003JB002941.
- Holtzman, B.K., Kohlstedt, D.L., Zimmerman, M.E., Heidelbach, F., Hiraga, T., Hufstoft, J., 2003. Melt segregation and strain partitioning: implications for seismic anisotropy and mantle flow. *Science* 301, 1227–1230.
- Holtzman, B.K., Kendall, J.-M., 2010. Organized melt, seismic anisotropy, and plate boundary lubrication. *Geochem. Geophys. Geosyst.* 11, Q0A06. doi:10.1029/2010GC003296.
- Jung, H., Mo, W., Green, H.W., 2009. Upper mantle seismic anisotropy resulting from pressure-induced slip transition in olivine. *Nat. Geosci.* 2, 73–77.
- Jung, H., Karato, S., 2001. Water-induced fabric transitions in olivine. *Science* 293, 1460–1463.
- Karato, S., 1989. Seismic anisotropy: mechanisms and tectonic implications. In: Karato, S., Toriumi, M. (Eds.), *Rheology of Solids and of the Earth*. Oxford University Press, pp. 393–422.
- Karato, S., 2008. Insights into the nature of plume–asthenosphere interaction from central Pacific geophysical anomalies. *Earth Planet. Sci. Lett.* 274, 234–240.
- Karato, S., Jung, H., Katayama, I., Skemer, P., 2008. Geodynamic significance of seismic anisotropy of the upper mantle: new insights from laboratory studies. *Annu. Rev. Earth Planet. Sci.* 36, 59–95.
- Kennett, B.L.N., Engdahl, E.R., Buland, R., 1995. Constraints on seismic velocities in the earth from travel times. *Geophys. J. Int.* 122, 108–124.
- Lebedev, S., van der Hilst, R.D., 2008. Global upper-mantle tomography with the automated multimode inversion of surface and S-wave forms. *Geophys. J. Int.* 173, 505–518. doi:10.1111/j.1365-246X.2008.03721.x.
- Levshin, A., Ratnikova, L., 1984. Apparent anisotropy in inhomogeneous media. *Geophys. J. R. Astr. Soc.* 76, 65–69.
- Lewis, J.L., Day, S.M., Magistrale, H., Castro, R.R., Astiz, L., Rebolgar, C., Eakins, J., Vernon, F.L., Brune, J.N., 2001. Crustal thickness of the peninsular ranges and Gulf Extensional Province in the Californias. *J. Geophys. Res.* 106 (B7), 13599–13611.
- Lizarralde, D., Axen, G.J., Brown, H.E., Fletcher, J.M., González-Fernández, A., Harding, A.J., Holbrook, W.S., Kent, G.M., Paramo, P., Suther, F., Umhoefer, P.J., 2007. Variation in styles of rifting in the Gulf of California. *Nature* 448, 466–469.
- Long, M.D., 2010. Frequency-dependent shear wave splitting and heterogeneous anisotropic structure beneath the Gulf of California region. *Phys. Earth Planet. Int.* 182, 59–72.
- Lonsdale, P., 1991. Structural patterns of the Pacific floor offshore of peninsular California. In: Dauphin, J.P., Simoneit, B.R.T. (Eds.), *The Gulf and peninsular province of the California*, AAPG Memoir 47, pp. 87–125.
- Lonsdale, P., 1989. Geology and tectonic history of the Gulf of California. In: Winterer, E.L., Hussong, D.M., Decker, R.W. (Eds.), *The Eastern Pacific Ocean and Hawaii, The Geology of North America*, volume N, pp. 499–521.
- López-Pineda, L., Rebolgar, C.J., Quintanar, L., 2007. Crustal thickness estimates for Baja California, Sonora and Sinaloa, Mexico, using disperse surface waves. *J. Geophys. Res.* 112, B04308. doi:10.1029/2005JB003899.
- Love, A.E.H., 1927. *A Treatise on the Theory of Elasticity*. Cambridge University Press, Cambridge, UK.
- Mainprice, D., Tommasi, A., Couvy, H., Cordier, P., Frost, D.J., 2005. Pressure sensitivity of olivine slip systems and seismic anisotropy of Earth's upper mantle. *Nature* 433, 731–733.
- Marone, F., Gung, Y., Romanowicz, B., 2007. Three-dimensional radial anisotropic structure of the North American upper mantle from inversion of surface waveform data. *Geophys. J. Int.* 171, 206–222. doi:10.1111/j.1365-246X.2007.03465.x.
- Meier, T., Dietrich, K., Stockhert, B., Harjes, H.P., 2004. One-dimensional models of shear wave velocity for the eastern Mediterranean obtained from the inversion of Rayleigh wave phase velocities and tectonic implications. *Geophys. J. Int.* 156, 45–58.
- Michaud, F., Royer, J.Y., Bourgois, J., Dymont, J., Calmus, T., Bandy, W., Sosson, M., Mortera-Gutiérrez, C., Sichler, B., Rebolledo-Viera, M., Pontoise, B., 2006. Oceanic-ridge subduction vs. slab break off: plate tectonic evolution along the Baja California Sur continental margin since 15 Ma. *Geology* 34, 13–16.
- Montagner, J.-P., 1998. Where can seismic anisotropy be detected in the Earth's mantle? *Pure Appl. Geophys.* 151, 223–256.
- Montagner, J.-P., 2002. Upper mantle low anisotropy channels below the Pacific Plate. *Earth Planet. Sci. Lett.* 202, 263–274.
- Nagy, E.A., Stock, J.M., 2000. Structural controls on the continent–ocean transition in the Northern Gulf of California. *J. Geophys. Res.* 105 (B7), 16251–16269.
- Nicholson, C., Sorlien, C.C., Atwater, T., Crowell, J.C., Luyendyk, B.P., 1994. Microplate capture, rotation of the western transverse ranges, and initiation of the San Andreas transform as a low angle fault system. *Geology* 22, 491–495.
- Nicolas, A., Christensen, N.L., 1987. Formation of anisotropy in upper mantle peridotite. In: Fuchs, K., Froidevaux, C. (Eds.), *Composition, Structure and Dynamics of the Lithosphere–Asthenosphere System*, pp. 111–123.
- Obrebski, M., Castro, R.R., Valenzuela, R.W., van Benthem, S., Rebolgar, C.J., 2006. Shear-wave splitting observations at the regions of northern Baja California and southern Basin and Range in Mexico. *Geophys. Res. Lett.* 33, L05302. doi:10.1029/2005GL024720.

- Obrebski, M., Castro, R.R., 2008. Seismic anisotropy in northern and central Gulf of California region, Mexico, from teleseismic receiver functions and new evidence of possible plate capture. *J. Geophys. Res.* 113, B03301. doi:10.1029/2007JB005156.
- Oskin, M., Stock, J., 2003. Miocene to Recent Pacific–North America plate motion and opening of the Upper Delfin Basin, northern Gulf of California, Mexico. *Geol. Soc. Am. Bull.* 115, 1173–1190.
- Paige, C., Saunders, M., 1982. LSQR: an algorithm for sparse linear equations and sparse least squares. *ACM Trans. Math. Softw.* 8, 43–71.
- Pallares, C., Maury, R.C., Bellon, H., Royer, J.Y., Calmus, T., Aguillón-Robles, A., Cotten, J., Benoit, M., Michaud, F., Bourgeois, J., 2007. Slab-tearing following ridge–trench collision: evidence from Miocene volcanism in Baja California, Mexico. *J. Volcanol. Geotherm. Res.* 161, 95–117. doi:10.1016/j.jvolgeores.2006.11.002.
- Persaud, P., Pérez-Campos, X., Clayton, R.W., 2007. Crustal thickness variations in the margins of the Gulf of California from receiver functions. *Geophys. J. Int.* 170. doi:10.1111/j.1365-246X.2007.03412.x, 687–669.
- Plattner, C., Malservisi, R., Dixon, T., Sella, G., Lafemina, P., Fletcher, J., Suarez-Vidal, F., 2007. New constraints on relative motion between the Pacific plate and Baja California microplate (Mexico) from GPS measurements. *Geophys. J. Int.* 170, 1373–1380. doi:10.1111/j.1365-246X.2007.03494.x.
- Sato, Y., 1955. Analysis of dispersed surface wave by means of Fourier Transform: Part 1. *Bull. Earthquake Res. Inst.* 33, 33–47.
- Severinghaus, J., Atwater, T.M., 1990. Cenozoic geometry and thermal state of the subducting slabs beneath North America. In: Wernicke, B.P. (Ed.), *Basin and Range Extensional Tectonics Near the Latitude of Las Vegas, Nevada*, *Geol. Soc. Amer. Memoir*, vol. 176, pp. 1–22.
- Sieminski, A., Paulssen, H., Trampert, J., Tromp, J., 2008. Finite-frequency SKS splitting: measurement and sensitivity kernels. *Bull. Seismol. Soc. Am.* 98, 1797–1810. doi:10.1785/0120070297.
- Smith, M.L., Dahlen, F.A., 1973. The azimuthal dependence of Love and Rayleigh wave propagation in a slightly anisotropic medium. *J. Geophys. Res.* 78, 3321–3333.
- Spencer, J., Normark, W., 1979. Tosco-Abreojos fault zone: a Neogene transform plate boundary within the Pacific margin of southern Baja California. *Geology* 7, 554–557.
- Spencer, J., Normark, W., 1989. Neogene plate-tectonic evolution of the Baja California Sur continental margin and the southern Gulf of California, Mexico. In: Winterer, E.L., Hussong, D.M., Decker, R.W. (Eds.), *The Eastern Pacific Ocean and Hawaii, The Geology of North America*, volume N, pp. 489–497.
- Stixrude, L., Lithgow-Bertelloni, C., 2005. Mineralogy and elasticity of the oceanic upper mantle: origin of the low-velocity zone. *J. Geophys. Res.* 110, B03204. doi:10.1029/2004JB002965.
- Stock, J.M., Hodges, K.V., 1989. Pre-Pliocene extension around the Gulf of California and the transfer of Baja California to the Pacific Plate. *Tectonics* 8 (1), 99–115.
- Süss, M.P., Shaw, J.H., 2003. P wave seismic velocity structure derived from sonic logs and industry reflection data in the Los Angeles basin, California. *J. Geophys. Res.* 108 (B3), 2170. doi:10.1029/2001JB001628.
- Trampert, J., Paulssen, H., van Wettum, A., Ritsema, J., Clayton, R., Castro, R., Rebollar, C., Perez-Vertti, A., 2003. New array monitors seismic activity near the Gulf of California in Mexico. *Eos Trans. AGU* 84 (4), 29–32.
- van Benthem, S.A.C., Valenzuela, R.W., Obrebski, M., Castro, R.R., 2008. Measurements of upper mantle shear wave anisotropy from stations around the southern Gulf of California. *Geophys. Int.* 47, 127–144.
- Visser, K., Trampert, J., Kennett, B.L.N., 2008. Global anisotropic phase velocity maps for higher mode Love and Rayleigh waves. *Geophys. J. Int.* 172, 1016–1032. doi:10.1111/j.1365-246X.2007.03685.x.
- Wang, Y., Forsyth, D.W., Savage, B., 2009. Convective upwelling in the mantle beneath the Gulf of California. *Nature* 462, 449–502.
- Zhang, X., Paulssen, H., Lebedev, S., Meier, T., 2007. Surface wave tomography of the Gulf of California. *Geophys. Res. Lett.* 34, L15305. doi:10.1029/2007GL030631.
- Zhang, X., Paulssen, H., Lebedev, S., Meier, T., 2009. 3D shear velocity structure beneath the Gulf of California from Rayleigh wave dispersion. *Earth Planet. Sci. Lett.* 279, 255–262.